Journal of Electrochemistry

Volume 24
Issue 5 *Special Issue for the Best Papers of the Award Winners in Electrochemistry*

2018-10-28

Design Strategies toward Highly Active Electrocatalysts for Oxygen Evolution Reaction

Tang TANG

Wen-jie JIANG

Shuai NIU

Jin-song HU

Recommended Citation
Tang TANG, Wen-jie JIANG, Shuai NIU, Jin-song HU. Design Strategies toward Highly Active Electrocatalysts for Oxygen Evolution Reaction[J]. *Journal of Electrochemistry*, 2018 , 24(5): 409-426.
DOI: 10.13208/j.electrochem.180146
Available at: https://jelectrochem.xmu.edu.cn/journal/vol24/iss5/2

DOI: 10.13208/j.electrochem.180146 **Artical ID**:1006-3471(2018)05-0409-18
Cite this: *J. Electrochem.* **2018**, *24*(5): 409-426 **Http**://electrochem.xmu.edu.cn

Design Strategies toward Highly Active Electrocatalysts for Oxygen Evolution Reaction

TANG Tang, JIANG Wen-jie, NIU Shuai, HU Jin-song*
(*CAS Key Laboratory of Molecular Nanostructure and Nanotechnology, CAS Research/Education Center for Excellence in Molecular Sciences, Institute of Chemistry, Chinese Academy of Sciences (CAS), Beijing* 100190, *China*)

Abstract: Electrocatalytic water splitting is pivotal for efficient and economical production of hydrogen and oxygen gasses. However, the efficiency of the whole device is largely limited by the oxygen evolution reaction (OER) at the anode due to its sluggish kinetics. Thus, it is imperative to develop inexpensive, highly active OER catalysts to lower the reaction barriers. By examining the underlying critical factors for OER performance, this review outlines general principles for designing efficient nanosized OER catalysts, including (1) enhancing the intrinsic activity of active site by electronic modulation, crystallinity modulation, phase control, defect engineering and spin state engineering; (2) designing appropriate micro/meso/macro structure with high electrical conductivity and mechanical stability to maximize the quantity of accessible active sites, and to promote electron transfer during OER process, as well as to achieve high durability especially at high current density. A series of highly efficient OER catalysts developed by our and other groups are then exemplified to demonstrate the guidance of these principles. At last, some perspectives are highlighted in the further development of efficient OER electrocatalysts, of which can contribute greatly to the achievement in large-scale commercialization of electrocatalytic water-splitting technology.

Key words: oxygen evolution reaction; water splitting; electrocatalysts; design principles; hydrogen production
CLC Number: O646 **Document Code**: A

The release of primary greenhouse gases such as carbon dioxide (CO_2) contributes greatly to the increase of global average surface air temperatures, disruption of weather patterns, and acidification of oceans [1-2]. The primary cause of this is human activity—most significantly, the intensive burning of fossil fuels, which leads to major concerns over the energy suppy, hence stimulating the development of clean energies over the past decades [3-5]. Generally, clean energies (solar, geothermal, wind power, and tidal energies) from natural sources can be converted into other forms such as electricity and chemical product/fuels for storage and resupply[6]. As a new type of storable and clean energy source, hydrogen molecule shows great potential in being an energy carrier as it is both carbon-free and environmentally friendly[7], thus playing a critical role in providing fuel or reactant for variety energy conversion and chemical process[8-10].

Electrocatalytic water splitting has been considered as one of the most mature technologies for high-purity hydrogen production except for other ways including natural gas reforming and biomass gasification[11-13]. This advanced technology can be distributed and combine with other renewable energy sources (solar, wind, etc.), showing a great potential in being an applicable technology for hydrogen production. Electrocatalytic water splitting consists of two half reactions including the hydrogen evolution reaction (HER) at the cathode and oxygen evolution reaction (OER) at the anode[14-15]. The commercial electrolyzer typically operates at a cell voltage of 1.8 ~ 2.0 V, which is much higher than the theoretical value of 1.229 V[8]. Thus, power consumption accounts for a large part of the cost by this technology. Therefore, it

Received: 2018-06-12, Revised: 2018-07-20 *Corresponding author, Tel: (86-10)82613929, E-mail: hujs@iccas.ac.cn

is critical to decrease the cell voltage of water splitting, reducing the cost of production and promoting its large-scale application.

The HER at the cathode proceeds through the reduction of water in two-electron pathway ($2H_2O + 2e \rightarrow H_{2(g)} + 2OH_{(aq)}^-$)[16-17]. In specific, the reaction primarily begins with the adsorption of a H_2O and a proton at the active site to form adsorbed H species and release a OH^- anion (Volmer reaction, step 1), followed by two possible reactions, namely, Tafel and Heyrovsky, respectively. For Volmer-Tafel route, this step includes another proton adsorption and recombination of the two adsorbed H species. For Volmer-Heyrovsky route, the adsorbed H species electrochemically desorb from the surface and react with an H^+ and a proton. This two paths end up with the desorption of hydrogen molecule[18-19]. Overpotential is present for every electrochemical reaction in reality[16]. Electrocatalyst is required to lower the overpotential, allowing the reaction to approach the thermodynamic equilibrium potential, and to promote the reaction rate and efficiency[16]. Currently, platinum (Pt)-group precious metals, nickel molybdenide (NiMo) and cobalt phosphide (CoP)-based non-precious metal materials have shown considerable HER activity with small overpotential of 10 ~ 50 mV to reach the current density of 10 $mA \cdot cm^{-2}$[7, 20-21]. However, the OER at the anode, described as $4OH^- \rightarrow 2H_2O + O_2 + 4e$ in basic solution, involves multistep proton-coupled electron transfer[22], leading to the significant sluggish kinetics in comparsion with HER. Therefore, the overpotential for OER is usually much higher than that for HER. Even using Ru- and Ir-based precious metal electrocatalysts, the overpotential can still be larger than 300 mV to deliver 10 $mA \cdot cm^{-2}$ for OER[23]. In other words, the efficiency of water splitting is largely limited by the OER at the anode[24-25]. Therefore, it is imperative to decrease the overpotential of OER to reduce the power consumption of electrocatalytic water splitting devices[26]. Accordingly, this review focuses on the development and design of efficient electrocatalysts for OER.

Generally, the state-of-the-art OER catalysts are the precious metal-based materials such as ruthenium (Ru) and iridium (Ir) oxides, which, also require large overpotentials to reach the desirable current densities[24]. Additionally, the scarcity of these metals in nature and the high cost of production into these catalysts limit their large scaled applications[27]. In the past decades, great advancements have been achieved in the manufacture of efficient OER catalysts. Some reports showed that the overpotential at 10 $mA \cdot cm^{-2}$ for OER could be decreased to be lower than 200 mV[26, 28]. However, there are still many problems to be solved, such as the real active sites of transition metal sulfides, selenides, and phosphides for OER, especially for multiple metals-based catalysts, where the role of each metal in catalyzing OER is still ambiguous. With that being said, it still remains to be challenging to fabricate cost-effective and efficient non-noble metal-based catalysts with high durability[14, 29].

1 OER Mechanism

It is generally accepted that the OER in a basic medium proceeds through five steps. The reaction begins with the adsorption and discharge of OH^- anions at the active site to form adsorbed OH species (step 1). Then followed by the reaction of OH^- with the adsorbed OH species to produce H_2O and an adsorbed atomic O, releasing an electron in the process (step 2). The third step involves the reaction of an OH^- anion with adsorbed O atom to form adsorbed OOH species (step 3), which then undergos reaction with additional OH^- anions (step 4), resulting in the formation of adsorbed O_2 and H_2O with the release of an electron. Adsorbed O_2 then desorbs from the active site to finish the overall reaction (step 5). Among the above five steps, the rate-limiting step is hypothesized to be step 3, i.e. the formation of OOH species[30]. According to the commonly accepted hypothesis based on the molecular orbital theory states, the intrinsic OER activities of transitional metal can be estimated by measuring their 3d orbital filling values from experiments[26, 31]. The 3d orbital filling values are related to the bond strength between the active sites and the reaction intermediate. Hence, a medium level of the orbital filling is indicative of neither a too strong nor a

too weak bond, which is beneficial for adsorption and desorption of OOH^- intermediate, hence promoting the overall reaction process. Therefore, a highly active site should have the suitble binding energy to facilitate the formation of OOH^-[31-32].

2 Research Status of OER Electrocatalysts

Over the last few years, transitional metals such as Fe, Co, Ni, Mn, Mo, and W have emerged as the most promising candidates to replace Ru- and Ir-based materials as they show relativily superior activity for OER in a basic medium. Tremendous efforts have been devoted to develop highly efficient and stable OER catalysts via tuning the composition such as metal oxides[30-31,33-35], hydroxides[14,27,29,36], chalcogenides[37-40], nitrides[41], and carbon-based materials[42-43]. To provide the meaningful comparisons in the catalytic activity and stability of these catalysts, as well as experimental evidence to aid or corroborate with the theoretical models of catalyst systems, a reliable method for measuring and reporting the performance of these materials under an identical condition should be applied. Jaramillo's group reported a benchmark protocol in measuring the activity, stability, and Faradaic efficiency of a series of representative OER catalysts in acid and alkaline media. This protocol was specifically developed to allow for the rapid screening of electrocatalytic performance through standard electrochemical procedures. Through electrodeposition, 23 kinds of non-noble metal uniform electrocatalyst films were prepared and evaluated. The overpotentials to achieve 10 mA·cm^{-2} were given after 2 h of constant polarization at 10 mA·cm^{-2} as shown in Figure 1A-B. In this work, none of the investigated non-noble metal catalysts were stable under OER condition in 1 mol·L^{-1} H_2SO_4 due to their thermodynamic instability of many transition metal oxides under oxidative potential in strong acid. In alkaline solution, most catalysts showed roughly equivalent activity for OER with overpotential of ~0.33 ~ 0.5 V to achieve 10 mA·cm^{-2}. A few catalysts exhibited relatively high activity and stability. NiMoFe-based catalyst film, for example, is the only non-noble metal catalyst that operates at 10 mA·cm^{-2} with an overpotential lower than 0.35 V. Futhermore, Markovic's group also established the overall catalytic activities

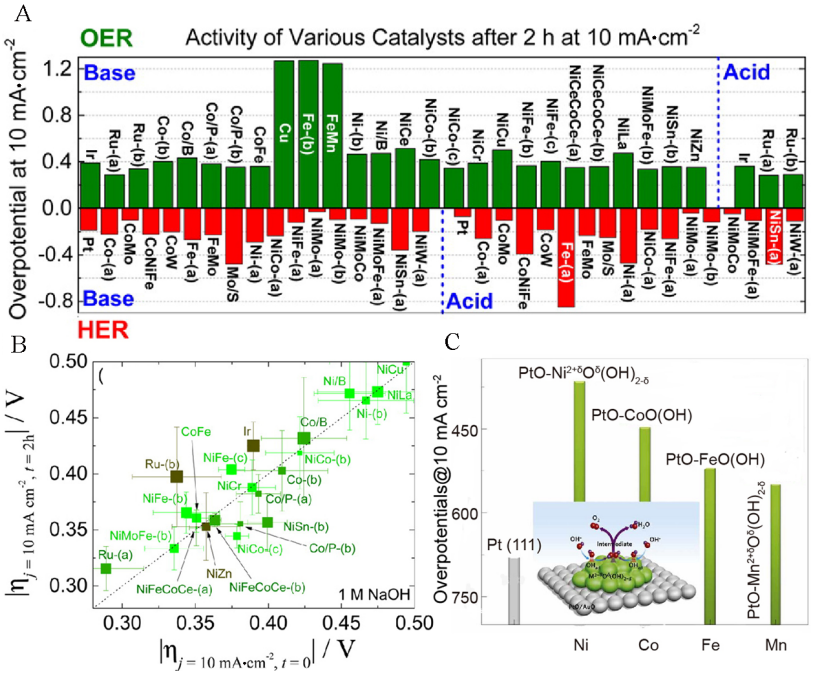

Fig. 1 (A) Activity diagrams of various catalysts after 2 h at 10 mA·cm^{-2} and (B) catalytic activity plots for alkaline OER performance. Copyright 2015 American Chemical Society. (C) Trend in overpotential for OER is shown as a function of the 3d transition elements. Copyright 2012 Nature publication.

of 3d-M metal hydr(oxy)oxides clusters modified Pt(111) electrodes with distinct stoichiometries and morphologies for OER as a function of a more fundamental property, a descriptor , OH-$M^{2+\delta}$ bond strength ($0 \leqslant \delta \leqslant 1.5$) as shown in Figure 1C[24]. This relationship exhibited the activity trend (Mn < Fe < Co < Ni), which is governed by the strength of the OH-$M^{2+\delta}$ energetic (Ni < Co < Fe < Mn). This indicates that Ni and Co-based electrocatalysts have the superior activity for OER among various transitional metals. These findings have stimulated the dramatic increase of research and work done on Ni or Co-based catalysts with various crystalline phases and nanoarchitectures[38, 44-49]. The successful identification of these electrocatalytic trends provides the foundation for rational design of active sites for practical alkaline OER electrocatalysts followed.

Although the great progress has been made in achieving highly active electrocatalysts for OER experimentally and theoretically, it is still imperative to further develop more efficient catalysts with lower overpotentials at a large scale.

3 Strategies for Enhancing OER Performance

OER process is one kind of heterogeneous reaction, which occurs at gas-solid-liquid three-phase-interface. From this, we can imply that the increase in number of accessible active sites can contribute to the design of efficient OER catalysts. Different from those heterogeneous chemical processes, electrochemical OER involves the electron transfer, which requires the high electron conductivity. Therefore, two strategies can be employed to enhance the activity of an OER catalyst system. One approach is through using the active sites with high intrinsic activity in OER catalyst, as shown in Scheme 1. It was reported that an well-performed catalyst could show a superior intrinsic activity of up to 10 orders of magnitude higher than the poor catalyst[3, 50]. Several methods have been reported to increase the intrinsic activity through creating highly active sites including electronic modulation[15, 39-40], crystallinity modulation[51], phase control[44], defect engineering[52], spin state engineering[53], etc. The second approach is through de signing nanosized electrode architectures. This strategy could improve the catalytic activity in the following aspects: (1) the nano-architecture with high surface area can increase the accessible active sites and facilitate the mass transportation during OER[15, 27, 46]; (2) the nanocomposites coupling active sites and conductive substrate such as graphene[14, 48], carbon nanotubes[47], nickel foams[15, 54], titanium foils[33, 55] can favor the efficient electron transfer; (3) good mechanical stability of the electrode can guarantee the electrochemical durability especially under large current density. These strategies are not mutually exclusive and could be unified in one catalystic system, thus jointly promoting the increase of catalytic performance. This review presents a series of highly efficient OER catalysts developed by our and other groups to demonstrate the guidance of these principles. Finally, conclusions and perspectives are highlighted on the development of more efficient OER electrocatalysts, which are the

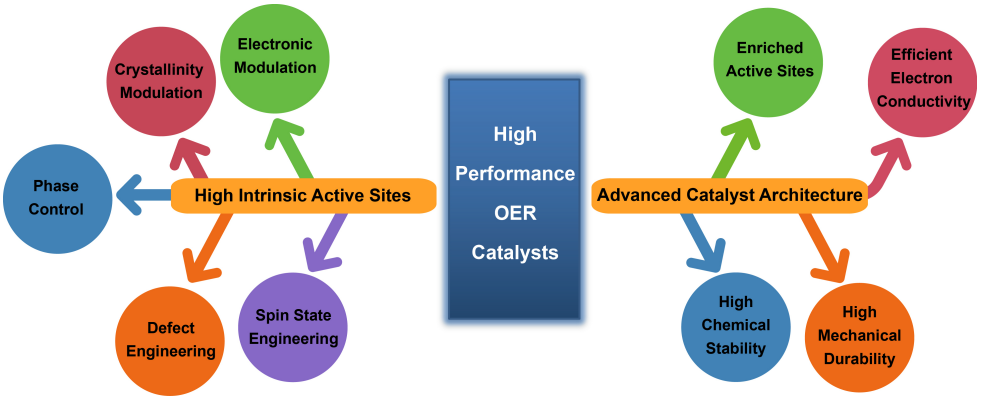

Scheme 1　Schematic illustration of the design strategies for high performance OER catalysts

key factors in accelerating the large-scale commercialization of electrocatalytic water-splitting technology.

3.1 Designing the Active Sites with High Intrinsic Activity

3.1.1 Electronic Modulation

Based on thereotical calculations, heteroatoms (cations or anions) doping and heterostructures between different materials or crystalline phases can efficiently modulate the electronic structure of the transition metal active sites, leading to a downward or rising shift of d-band center, and thus, a weakened or strengthened adsorption of intermediate species such as the OOH^*[3, 28, 31]. As a result, the catalytic activities of active site can be adjusted. Our group found that Mn doping can enhance the performance of Co active center in Co carbonate hydroxide (CoCH)[32]. The possible affect caused by the change of the morphology and ECSA of CoCH by Mn doping was eliminated by cation exchange. The obtained sample was denoted as CoMnCH-ce. The energy-dispersive X-ray spectroscopic (EDS) spectra in Figure 2A verified that the deliberate incorporation of Mn ions into CoCH has not changed its morphology and electrochemical surface area (ECSA) (Figure 2B). However, CoMnCH-ce exhibited an obvious enhanced OER performance with an overpotential of 356 mV at 50 mA·cm^{-2} compared with 380 mV for CoCH (Figure 2C). Such an activity enhancement should be attributed to the improvement of intrinsic activity of active sites by Mn incorporation. X-ray photoelectron spectroscopic (XPS) data in Figure 2D shows that the binding energy of Co sites in CoMnCH-ce shifted downwards by 0.70 eV (780.87 vs. 781.57 eV), suggesting that Mn doping can appreciably modulate the electronic structure of Co centers. Density of states (DOS) calculations suggested that the Co 3d orbital for CoMnCH has showed a negative shift compared to that for undoped CoCH, indicating that the Mn doping lowered the energy of Co atoms and enabled Co atoms to gain more electrons (Figure 2E). DOS profiles were then integrated to give the average electron number in 3d orbital per Co atom in these structures, as shown in Figure 2F. The electron number in 3d orbital of Co atom in CoCH was about 7.15 (theoretical value for Co^{2+} is 7), which is lower than 7.30 of that in CoMnCH. This change was well consistent with the lower of binding energy of Co $2p_{3/2}$ for CoMnCH (Figure 2D).

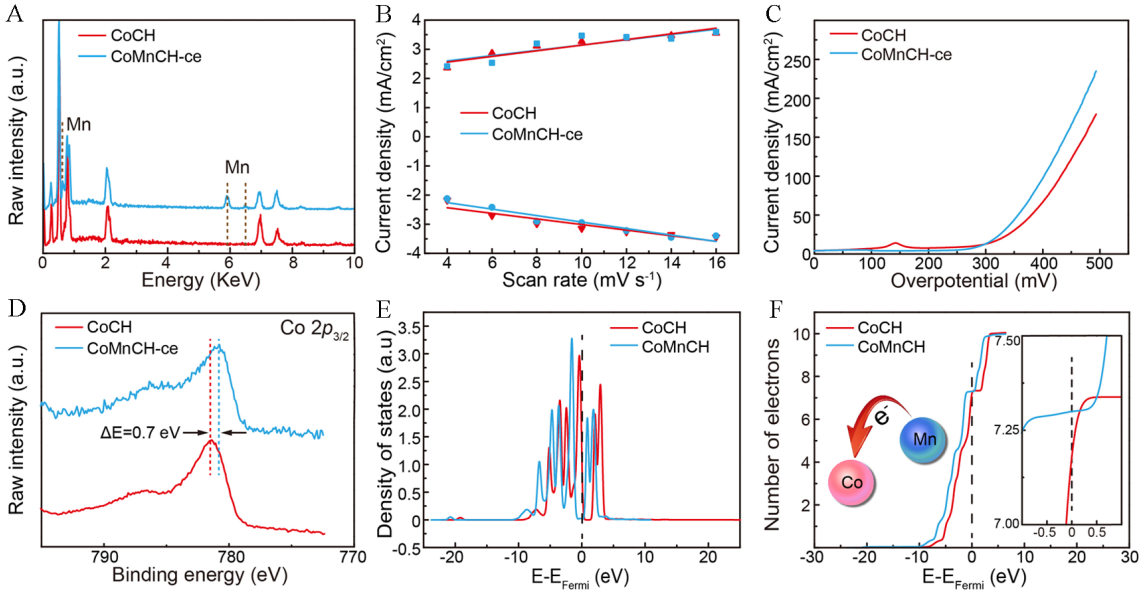

Fig. 2 (A) EDS spectra. (B) ECSA evaluation. (C) OER polarization curves without iR-compensation. (D) Co $2p_{3/2}$ spectra of CoCH and CoMnCH-ce. (E) DOS of Co 3d orbital and (F) corresponding number of electrons in the 3d orbital per Co atom in CoCH and CoMnCH. Copyright 2017 Amercian Chemical Society.

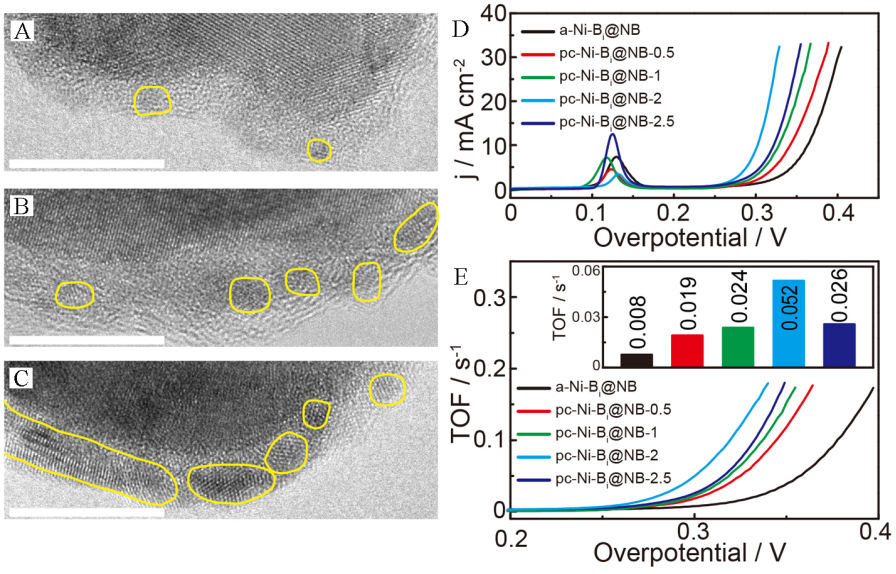

Fig. 3 (A-C) TEM images of pc-Ni-Bi@NB with different crystallinities. The scale bars are 10 nm. (D) OER polarization curves and (E) TOF per oxidative nickel site (Ni^{2+}) for a-Ni-Bi@NB and pc-Ni-Bi@NB catalysts. The inset in (E) shows the TOF values at the overpotential of 300 mV. Copyright 2017 Wiley-VCH.

The increase in number of electrons in Co 3d orbital for CoMnCH could benefit the formation of adsorbed OOH species, and thus facilitate the OER process[40,56].

3.1.2 Crystallinity Modulation

Commonly, the highly crystalline catalysts with strong crystal lattice constraint could promote the stable catalytic activity during operation. However, OER only occurs on the surface of catalysts and non-ions could penetrate the bulk of catalysts, leading to the low efficiency. On the contrary, amorphous catalysts with a weak ligand environment could facilate the change of valency state of the catalytic species and could expose those highly active sites including grain boundaries, point and line defects, undercoordinated sites, and edge at steps or kinks. It was reporetd that the electrocatalysts in amorphous state exhibited better activity than those in crystalline one[57]. Deliberately tuning the crystallinity of electrocatalysts and investigating the influence on catalytic activity could offer an alternative way to improve the electrochemical performance. Our group reported an OER catalyst with nickel boride (NB) nanoparticles as cores and nickel borate (Ni-Bi) as shells, denoted as Ni-Bi@NB, via a very simple and facile aqueous reaction[51]. It was intriguingly found that the crystallinity of Ni-Bi shells could be efficiently modulated by annealing at the same temperature for different time as shown in Figure 3A-C and the OER activity of Ni-Bi is closely dependent on its crystallinity. The partially crystalline Ni-Bi (pc-Ni-Bi@NB) exhibited the much higher activity than amorphous or crystalline one (Figure 3D). The amorphous a-Ni-Bi@NB showed the worst OER activity in terms of exhibiting the largest overpotential. With the increase of annealing time from 0.5, to 1 and 2 h, the overpotentials at 10 mA·cm^{-2} gradually decreased from 341 to 328 to 302 mV, implying that the initial improvement in the crystallinity of Ni-Bi due to annealing enhances OER activity. However, when the annealing time extended to 2.5 h, the OER overpotential increased to 322 mV, indicating that the further improvement in the crystallinity of Ni-Bi downgraded the OER performance. The turnover frequencies (TOF) were also calculated as shown in Figure 3E. The pc-Ni-Bi@NB-2 exhibited the highest TOF value of 0.052 s^{-1}, which is nearly seven times higher than the 0.008 s^{-1} for a-Ni-Bi@NB. However, the value of pc-Ni-Bi@NB-2.5 decreased to 0.026 s^{-1}. The apparent differences in OER activity of Ni-Bi@NB samples mainly originate from the differences in the intrinsic activity of active sites in

Ni-Bi with different crystallinities. The partially crystallized Ni-Bi shell, in this case, is expected to expose more highly active sites as mentioned above.

3.1.3 Phase Control

Chemical compounds with different crystalline phases have different electronic states and physical properties, thus, exhibit totally different catalytic activities. A well-known example is cobalt disulfide (MoS_2) with 2H phase being semiconductor, while 1T phase metallic. These two different MoS_2 showed distinct intrinsic activity for HER[58]. Also, Wu's group reported the phase-transformation engineering for cobalt diselenide ($MoSe_2$) can be realizing enhanced HER performance, it is found that different Co-Se bond lengths have different H atom and water molecule adsorption energies, thus bringing the possibility to enhance the HER performance by adjusting the phase between cubic pyrite-type and orthorhombic marcasite-type $CoSe_2$[59]. Therefore, the phase control could effectively adjust the electronic state of active sites in the same compound and achieve highly active materials for OER. Yan's group reported active and stable α-$Ni(OH)_2$ hollow spheres for OER with a small over potential of 0.331 V at a current density of 10 mA·cm^{-2} and a small Tafel slope of ~ 42 mV·decade^{-1} as shown in Figure 4, comparing favorably with the state-of-the-art RuO_2 catalyst[44]. Additionally, two β-$Ni(OH)_2$ catalysts with morpholoies of nanoplates and nanoparticles were also prepared. The β-$Ni(OH)_2$ nanoplates exhibited a large overpotential of 0.44 V to reach 10 mA·cm^{-2} and the β-$Ni(OH)_2$ nanoparticles even failed to reach such current density. The intrinsic activities of above catalysts were further estimated by TOF by assuming every metal atom is to be catalytically active. It was found that the α-$Ni(OH)_2$ catalyst exhibited the highest TOF of ~ 3.61 × 10^{-2} s^{-1} at an overpotential of 0.35 V, which is ~12 times higher than the β-$Ni(OH)_2$ nanoplates did. The superior OER activity of α-$Ni(OH)_2$ could be attributed to the *in-situ* formation of active γ-NiOOH phase, where highly oxidized Ni can facilitate the formation of OOH species and subsequent conversion of oxygen.

3.1.4 Defect Engineering

The surface properties of nanomaterials play a key role in achieving highly active electrocatalysts. Defects on surface including point defects, line defects, plane defects, and volume defects can tune the electronic and surface properties, which are common-

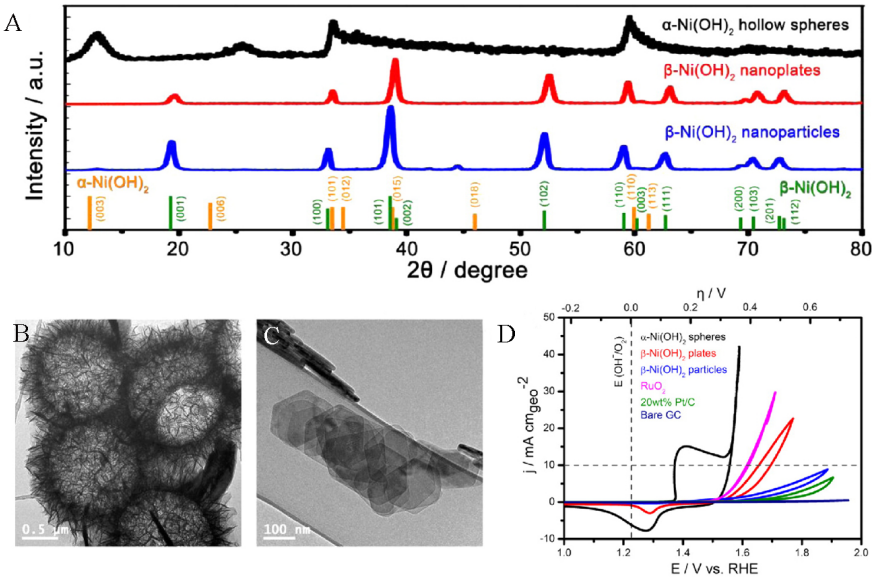

Fig. 4 (A) XRD patterns for α-$Ni(OH)_2$ hollow spheres, β-$Ni(OH)_2$ nanoplates, and β-$Ni(OH)_2$ nanoparticles. TEM images of (B) α-$Ni(OH)_2$ hollow spheres and (C) β-$Ni(OH)_2$ nanoplates. (D) CVs recorded at 100th cycle for bare GC electrode and modified GC electrodes comprising the α- and β-$Ni(OH)_2$, RuO_2, and 20wt% Pt/C. Copyright 2014 Amercian Chemical Society.

ly thought to play an important role in catalyzing OER[38, 52]. For example, the existence of oxygen vacancies in metal oxides can effectively adjust the bandgap of semiconductors or change the distribution of electrons on the surfaces of materials[60]. There are numerous reports showing how the defects in spinel and perovskite oxides can greatly improve the OER performance[61]. Zheng's group reported the reduced mesoporous Co_3O_4 nanowires (NWs) with abundant oxygen vacancies for OER, showing an enhanced performance[62]. This fabrication process is shown in Figure 5A, the pristine mesoporous Co_3O_4 NWs were treated with $NaBH_4$ at room temperature to reduce Co_3O_4 NWs forming oxygen vacancies. The partial charge density was calculated to better understand the oxygen vacancies states as shown in Figure 5B. The distribution of the two electrons previously associated with the three Co-O bonds is displayed in yellow. It can be clearly seen that the two electrons that previously occupied the oxygen 2p orbitals became delocalized around the adjacent three Co^{3+} atoms and the O atoms after losing an oxygen atom, which would increase the degree of electron delocalization from the pristine situation. The obtained conductivity of the reduced Co_3O_4 is much higher than that of the pristine Co_3O_4. DOS calculation was used to further investigate the positive role of the oxygen vacancies in the electrocatalytic performance, as shown in Figure 5C. Reduced Co_3O_4 showed the formation of a new state within the band gap located at about 1.1 eV below the conduction band minimum, which mainly contributes to Co^{3+} 3d (and a small amount of O 2p) states. Besides, theoretical calculation showed the formation energy of oxygen vacancies for reduced Co_3O_4 is low, indicating that more oxygen vacancies are asscioated with higher oxygen releasing capability. The reduced Co_3O_4 NWs showed a current density of 13.1 mA·cm^{-2} for OER (Figure 5D), about over 7 times higher than the pristine Co_3O_4 NWs. Both the experimental and theoretical results showed that the oxygen vacancies produced by $NaBH_4$ reduction contributed to improving the OER activity. Such method

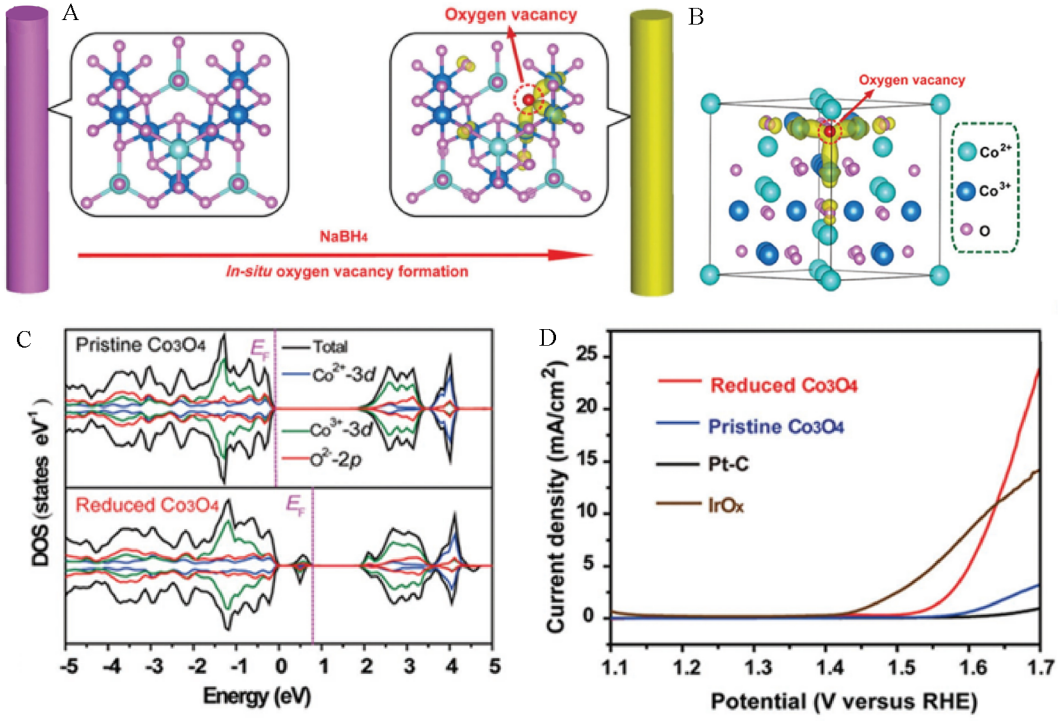

Fig. 5 (A) Schematic illustration of the $NaBH_4$ reduction for *in-situ* creation of oxygen vacancies in Co_3O_4 NWs. (B) Partial charge density of the reduced Co_3O_4. (C) TDOS and PDOSs of the pristine Co_3O_4 and reduced Co_3O_4 (with oxygen vacancies). (D) LSV currents of the reduced Co_3O_4 NWs, pristine Co_3O_4 NWs, IrO_x, and Pt/C. Copyright 2014 Wiley-VCH.

is facile and robust, and does not require high-temperature treatment. This may enable a unique approach to produce oxygen vacancies in semiconductor oxides at an atomic level, which can substantially enhance the electrochemical and catalytic performance for a large variety of other materials.

3.1.5 Spin State Engineering

The modulation of electronic configuration could be a general and effective strategy for improving intrinsic OER activity. The spin state is directly related to the occupancy of e_g orbital of transition metals in their compounds, governing many pivotal reaction steps including OER. Spin state engineering as an important regulative method is discovered in perovskite-based electrocatalysts by Yang's group[9]. Subsequently, Wu's group recently reported a unique spin-state regulation method to optimize oxygen evolution activity by lattice-oriented control of $LaCoO_3$ epitaxial film[63]. As shown in Figure 6A, the proportions in low spin (LS) state for $LaCO_3$ (100), (110), and (111) films are 87%, 48% and 31%, respectively, which indicates that the number of unpaired average electrons (e_g electrons) of $LaCO_3$ (100), (110) and (111) films were 0.87, 0.48, and 0.31, respectively (Figure 6B). X-ray absorption near edge structure (XANES) results (Figure 6C) indicate that the transition of some electrons in t_{2g} orbitals fills in the e_g orbitals, leading to the electronic redistribution between e_g and t_{2g} levels and giving rise to the partially unoccupied t_{2g} states of cobalt ions to reach an intermediate spin state (LS $t_{2g}^5e_g^1$). As expected, $LaCO_3$ (110) film possesses better OER performance than other two films (Figure 6D). This high performance comes from the optimized e_g electron, and thus, a lower adsorption free energy and higher conductivity (Figure 6E). Xie's group also reported the engineering of spin states in ultrathin Co_3S_4 nanosheets[53]. The atomically thin Co_3S_4 nanosheets (denoted as CSATN)

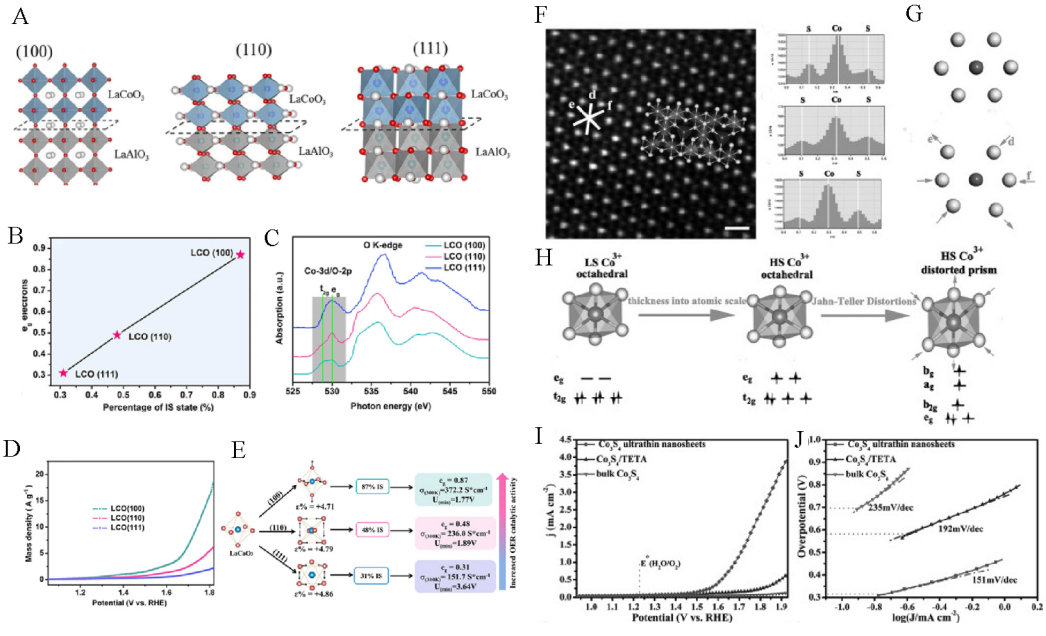

Fig. 6 (A) Schematic illustration of the as-prepared $LaCO_3$ (100), (110), and (111) films. (B) Average e_g electrons of different oriented $LaCO_3$ films. (C) O K-edge XANES spectra for $LaCO_3$ (100), (110), and (111) films. (D) The OER polarization curves of the $LaCO_3$ films. (E) The relationship between OER activity and spin configuration (free energy, conductivity as well as e_g electrons filling status) of differently oriented $LaCO_3$ films. Copyright 2017 Cell Press. (F) HAADF image of CSATN (scale bars 0.5 nm) and HAADF intensity line profiles along the directions signed by the white lines in HAADF image. (G)[111] zone axis section view of original octahedral and Jahn-Teller distortion. (H) Representations of structural transformation by reducing its thickness to the atomic scale. (I-J) LSV polarization curves and corresponding Tafel plots of as-prepared materials. Copyright 2015 Wiley-VCH.

could be rationally manufactured by ultrasound exfoliation treatment from an intermediate Co_3S_4/TETA (TETA = triethylenetetramine) hybrid precursor as shown in Figure 6F-J. The sole exposure of octahedral coordination cations in CSATN was confirmed by high-angel annular dark field (HAADF) image, suggesting the presence of Jahn-Teller effect of Co-S_6 octahedral. Temperature-dependent electron paramagnetic resonance (EPR) data revealed that single low spin Co^{2+} signal without Co^{3+} signal in bulk Co_3S_4 and the Co^{3+} in CSATN manifested a high spin state. High spin Co^{3+} in octahedral ($t_{2g}^4e_g^2$) will distort to remove the degeneracy and form a lower energy system, further confirming the Jahn-Teller effect from HAADF result. As a result, the synergistically engineering spin states and the expousure of polyhedral in ultrathin nanosheets endowed the CSATN with superior OER performance in neutral solution compared with the bulk one. Additionally, Wei's group reported that the γ-CoOOH nanosheets with thickness of 1.4 nm showed 20 times higher of OER performance than bulk one[64]. Experimental characterizations and first-principles calculations provide solid evidence of the half-metallic nature of the as-prepared nanosheets with local structure distortion of the surface CoO_{6-x} octahedron. When bulk γ-CoOOH was decreased to atomic thickness, the electronic state of Co 3d orbital changed from $t_{2g}^6e_g^0$ configuration to $t_{2g}^5e_g^{1.2}$ configuration. The increased hole state in the t_{2g} orbital of CoO_{6-x} octahedron can enhance the electrophilicity of the adsorbed O and facilitate the adsorption of the hydroxyl group on the catalytically active sites to form adsorbed -OOH species. Besides, the σ-bonding e_g orbital has a stronger ability to overlap with the oxygen-related adsorbate than the π-bonding t_{2g} orbital, it can promote electron transfer between surface cation (CoO_{6-x}) and adsorbed -OOH intermediates more directly. These natures induced by two-dimension confinement in the γ-CoOOH contributed to the higher catalytic activity of γ-CoOOH nanosheets.

3.2 Designing Architecture for Hosting Active Sites

3.2.1 Active Sites Enrichment

Aside from increasing the intrinsic activity of each active site, increasing the number of accessible active sites on a given electrode is another effective way to improve OER performance. It was reported that the performance can be increased up to 3 orders of magnitude by increasing the catalyst loading or optimizing the architecture of electrode[3, 50]. Therefore, rational design of catalyst structure is known to be crucial for improving the electrode performance. In the pursuit of creating large surface area and high active site density, various attempts have been devoted to developing three dimensional (3D) nanostructured catalyst materials. Nickel foam (NF) materials typically have extra-large macropores, providing enormous open space to build up more dedicated nanostructures with multiple levels of porosity to further enhance specific surface area without affecting the gas bubble dissipation of NF. Zhao's group reported a porous architecture for NiFe-based catalysts through *in-situ* growing vertically aligned $NiCo_2O_4$ nanoflakes onto NF before the topmost NiFe nanosheets are electrodeposited (denoted as NiFe/$NiCo_2O_4$/NF)[48]. As shown in Figure 7A-B, this electrode is comprised of three levels of porous structures including the bottom supermacroporous Ni foam ($\approx$ 500 μm) substrate, the intermediate layer of vertically aligned microporous $NiCO_2O_4$ nanoflakes ($\approx$ 500 nm), and the topmost NiFe(oxy) hydroxide mesoporous nanosheets ($\approx$ 5 nm). This hierarchical architecture is binder-free and beneficial for exposing catalytic active sites, enhancing mass transport and accelerating dissipation of gases generated during OER. The as-prepared NiFe/$NiCo_2O_4$/NF electrode displayed a significantly enhanced OER catalytic activity, compared to NiFe/NF electrode (without intermediate layer of $NiCo_2O_4$ nanoflakes), $NiCo_2O_4$/NF electrode (without topmost layer of NiFe nanosheets), and bare NF, with an onset potential of about 1.47 V and an overpotential of 340 mV to deliver an extremely large current density of 1200 $mA \cdot cm^{-2}$ (Figure 7C). The multilevel hierarchical architecture offers significantly enhanced accessible surface area and a large number of active sites, thus greatly promoting the OER performance. Our group

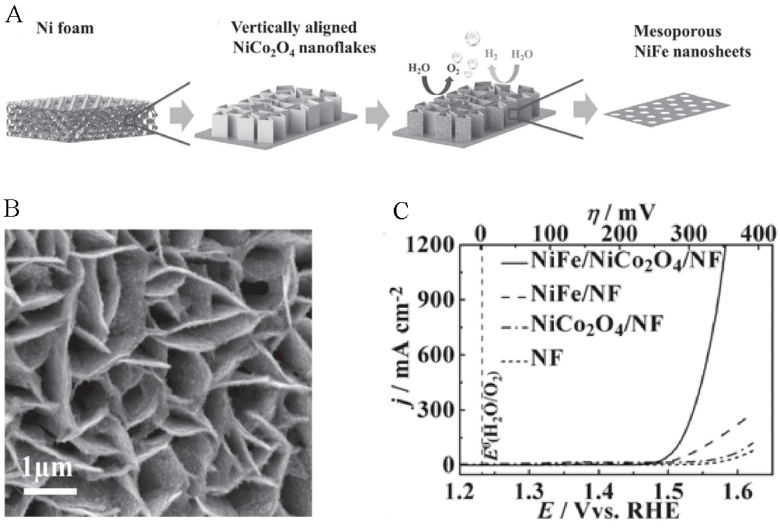

Fig. 7 (A) Schematic illustration showing the formation process of porous NiFe/$NiCO_2O_4$/NF composite electrodes. (B) SEM image of NiFe/$NiCO_2O_4$/NF electrode. (C) OER polarization curves of NiFe/$NiCO_2O_4$/NF, NiFe/NF, $NiCO_2O_4$/NF, and NF in 1 mol·L^{-1} KOH. Copyright 2016, Wiley-VCH.

found that the direct growth of cobalt carbonate hydroxide nanosheets (CoCH) on NF and the morphology could be effectively modulated by Mn element doping[15]. The electrochemical surface area (ECSA) of Co_xMn_yCH samples could be increased from 92.7 mF·cm^{-2} for pure CoCH to the top value of 380.2 mF·cm^{-2} for Co_1Mn_1CH. As a result, the optimized Co_1Mn_1CH exhibited much improved OER activity with a low overpotential of 294 mV at 30 mA·cm^{-2}, compared to 337 mV for pristine CoCH. The impressing catalytic performance could be attributed to the large quantity of accessible active sites induced by Mn doping.

3.2.2 Efficient Electron Conductivity

The OER proceeds through four-step proton-coupled electron transfer. Thus enough conductivity of OER catalysts is necessary for the efficient electron transfer during OER[65-66]. A few materials such as metal ox ides and hydroxides possess high in trinsic catalytic activity but suffer from low electronic conductivity, seriously lowering their apparent catalytic activities for OER and limiting their practical utilization at large output. Coupling these materi als with high conductive substrates such as carbon materials (CNTs, graphene) and metal electrode (nickel foam) was proven as an effective way to improve their low electron transfer ability[30, 67-68]. Graphene was used to take advantage of its high conductivity and large surface area to demonstrate this improvement[46, 69-74]. Our group developed a kinetically controlled room-temperature coprecipitation to produce sandwich-type α-phase nickel cobalt hydroxides nanosheets/graphene composites (NiCo-HS@G) as shown in Figure 8A[75]. The hydroxide nanosheets were aligning on the graphene layer to form an interconnected nanowall-like structure for NiCo-HS@G (Figure 8B-C). While without the graphene skeleton (denoted as NiCo-HS), hydroxide nanosheets self-nucleated and assembled into irregular particles in a size of hundreds of nanometres (Figure 8D). The hierarchal structure of NiCo-HS@G not only effectively prevented the agglomeration of graphene layers, but also enhanced the structure stability and the intimate contact between the nanosheets and graphene layers, guarantying the efficient electron transfer and high durability during electrochemical operation. Electrochemical impedance spectroscopic (EIS) measurements showed a significantly distinct charge transfer resistances (R_{ct}). In Fig. 8E, the NiCo-HS@G catalyst showed the smallest R_{ct} value of about 16 Ω among the values of 170 Ω for NiCo-HS and 1078 Ω for bare graphene, indicating the fastest electron transfer kinetics of

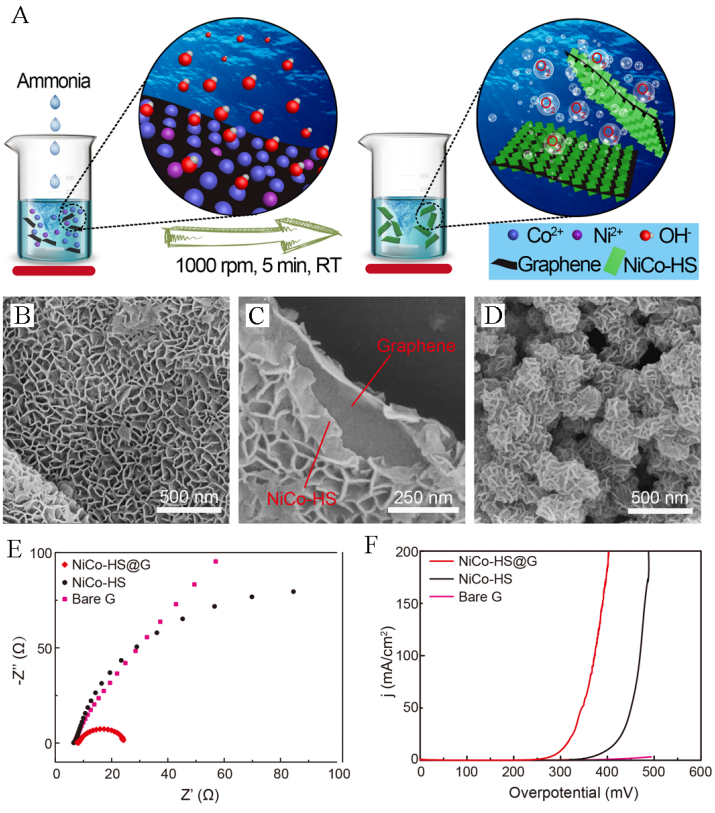

Fig. 8 (A) Schematic illustration of the fabrication process of NiCo-HS@G. SEM images of (B-C) NiCo-HS@G and (D) NiCo-HS. (E) EIS Nyquist plots at 1.53 V (vs. RHE) and (F) OER polarization curves with 90% iR-compensation of NiCo-HS@G, NiCo-HS, and bare graphene. Copyright 2018, Wiley-VCH.

NiCo-HS@G. A four-probe resistance measurement was carried to measure the powder electronic conductivity values of NiCo-HS and NiCo-HS@G in order to gain further insight of the effect of graphene skeleton on the charge-transfer process. The NiCo-HS@G exhibits a conductivity of 4.7×10^{-4} S·cm^{-1}, which is 2 orders of magnitude higher than 6.9×10^{-6} S·cm^{-1} of NiCo-HS. Such increase in the conductivity would facilitate the electron transfer during OER, thus enhancing its electrochemical activity. As shown in Figure 8F, NiCo-HS@G delivered a current density of 10 mA·cm^{-2} at a low overpotential of 302 mV, which is much smaller than 399 mV of NiCo-HS. The superior performance originated from the tight contact between NiCo-HS and graphene, promising effective electron transfer. Similarly, a strong-coupled cobalt borate nanosheets/graphene hybrid was also developed through a room-temperature chemical route, the strong synergetic coupled effect tightly anchoring cobalt borate nanosheets on the graphene surface, thus, achieve enhanced electron transfer capacity and also provide high surface active sites exposure yield, and eventually promote OER performance at both alkaline and neutral conditions[76]. These findings indicate that incorporating conductive materials could be an effective way to improve electron transfer and mass transportation during OER.

3.2.3 High Durability at Large Current Density

In addition to catalytic activity, long-term stability especially at large current density is another metric for a practical OER catalyst. To date, most of reported catalysts are powders for basic scientific exploration, which were evaluated by coating on conductive substrate with polymeric binders. In practical application, OER would usually proceede under harsh conditions such as at high current density. In this case, the current density of OER could be interfered from high-flux oxygen evolution and even the active components in OER electrode would peel off, fast degrading the overall performance of water splitting de-

vice[77]. Therefore, electrochemial and mechanical stabilities of OER catalysts are required to fulfill the criteria for real application. *In-situ* growing active materials on highly conductive substrate could guarantee the tight contact between them, producing stable electrode of OER especially for water splitting at high current density[3, 78]. Our group reported *in-situ* aligning growth of $Ni(OH)_2$ nanoplates on NiAl alloy foil (denoted as $Ni(OH)_2$/NiAl) by simply dealloying NiAl foil in KOH solution (Figure 9A-B)[79]. NiAl foil substrate is low-cost, commercially available, and physically robust. The aluminum is amphoteric and ease to be etched away in alkaline solution to form hierarchically porous structure on NiAl foils, accompanying with the *in-situ* growth of $Ni(OH)_2$ nanoplate arrays. Such hierarchical $Ni(OH)_2$/NiAl could act as an active and robust scaffold for the electrodeposition of other catalysts with intrinsically higher activity such as NiFe nanoparticles to further enhance the OER performance (Figure 9C). The as-prepared NiFe/$Ni(OH)_2$/NiAl displays superior OER catalytic activity with overpotentials of 246, 315, and 374 mV at 10, 100, and 500 mA·cm^{-2}, respectively (Figure 9D). Notably, the NiFe/$Ni(OH)_2$/NiAl electrode was tested at a high current density of 250 mA·cm^{-2} for 10 h, the overpotential increased by only 20 mV as shown in Figure 9E. The good durability could be attributed to the stable hierarchical $Ni(OH)_2$/NiAl scaffold. Cao's group reported an autologous growth strategy to prepare grown metal hydroxides on NF surfaces, and then to inject Fe component by ion-exchange[80]. The resulted electrode was denoted as Fe:$Ni(OH)_2$/NF, which exhibited very high catalytic activity with an overpotential of 325 mV at 1000 mA·cm^{-2}. This electrode was tested under 1200 mA·cm^{-2} with the violent evolution of O_2 bubbles for near 50 h and nearly no performance attenuation was observed. After such harsh stability test, the electrode was subjected to various characterizations. The morphologies and surface contents of Ni and Fe remained almost unchanged, which further confirmed its outstanding robustness. These examples indicate that *in-situ* growing active materials on highly conductive substrate can efficiently fabricate excellent stable electrode for practical water splitting system at large current density.

Aside from the mechanical durability, the chemical stability is also very important since the currently reported highly perforamance metal sulfides and selenides for OER are known to be not stable in basic solutions. Recently, Jin's group disscussed wheather metal chalcogenides, nitrides, and phosphides are real

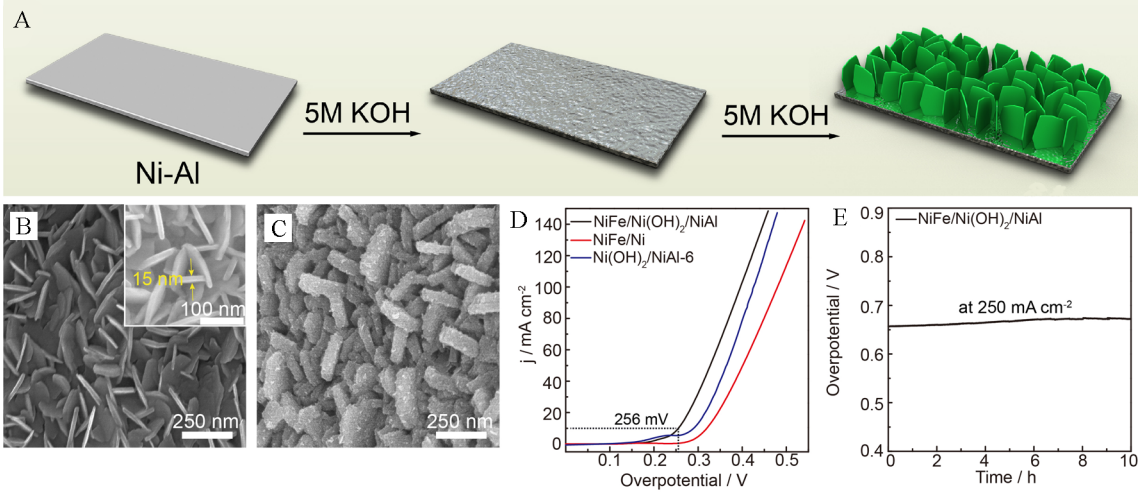

Fig. 9 (A) Schematic illustration of the fabrication process of $Ni(OH)_2$/NiAl. SEM images of (B) $Ni(OH)_2$/NiAl (The inset is high-resolution SEM image) and (C) NiFe/$Ni(OH)_2$/NiAl. (D) LSV curves for as-prepared catalysts at a scan rate of 5 mV·s^{-1} for OER. (F) Chronopotentiometric curve recorded on NiFe/$Ni(OH)_2$/NiAl at a constant current density of 250 mA·cm^{-2}. All curves were recorded without iR-correction. Copyright 2017 Wiley-VCH.

OER catalysts[81], in which these compounds are considered to be not stable and will be oxidated to a core-shell structure composed of a MO_x/$M(OH)_x$ shell outer the original core. The as-prepared metal sulfides and selenides often display apparent electrocatalytic performance better than those of the corresponding metal oxides and hydorxides, which may be attributed to the derived metal oxides/hydorxides with high surface area and thus boost the catalytic activity. Wu's group reported an electrochemical activation of Co_2P in alkine media for enahnced OER perormance[82]. The electrochemical activation in hash media could easily break the strong Co-Co bond and promote active species generation on the surface of metallic Co_2P. The as-formed amorphous metal oxo-/hydroxides provided highly active sites for OER. HRTEM and EDX results indicate that an amorphous metal oxo-/hydroxides were formed on the surface of normal Co_2P particles after OER tests. The difference between activated and normal Co_2P is the different layer thickness. The activated Co_2P showed a much thicker layer. Similar phenomenon can also be obseved on CoP nanoparticles and Ni_2P nanoparticles.

4 Conclusions and Perspectives

By examining the underlying critical factors, this review systematically summaries the design methodology for constructing high performance OER catalysts. Generally, there are two main approaches: Enhancing the intrinsic activity of active sites and designing proper micro/meso/macro structure with high electronic conductivity and mechanical stability. The first strategy could be achieved through electronic modulation (usually cation or anion doping), crystallinity modulation, phase control, defect engineering, and spin state engineering. The above metioned methods work in correlation instead of independently. For example, crystallinity modulation on a catalyst would lead to the formation of grain boundaries, point and line defects, undercoordinated sites, and edge at steps or kinks. These high intrinsic active sites could be also produced by the mothod of defect engineering. The methods of phase control, defect engineering, and spin state engineering would inevitably alter the electronic state of active sites in catalysts, which is in coorelation with electronic modulation. This review did not go in depth instead simply discussed the commonly reported approachs to enhance the intrinsic activity of active sites. The underlying connections of these methods were also not specified herein. The second strategy maximizes the quantity of accessible active sites, promoting electron transfer during OER process as well as achieving excellent durability especially at high current density. The two strategies mentioned are not mutually exclusive and could be unified in one catalyst system, thus jointly promoting the increase of catalytic performance.

Although these strategies have been widely applied to improve the OER performance, there are still other challenges presented, which remains to be overcomed. To begin with, a large number of highly efficient electrocatalysts based on metal sulfides, selenides, and nitrides have been reported to exhibit much higher activities than the corresponding metal oxides and hydroxides. However, due to the easily oxidation of these materials under alkaline OER conditions, metal (oxy)hydroxides would be formed. It is those newly evolved species are reported to be the real catalytically active sites in metal sulfides, selenides, and nitrides for OER. The issue lies in that reason for the significant difference of catalytic activity among metal oxides, hydroxides and metal sulfides, selenides, nitrides is not fully understood yet. In the past decades, advanced *in-situ* physical/chemical characterization techniques (aberration-corrected TEM, X-ray absorption spectroscopy, *in-situ* XPS, etc.) have made great achievements. These techniques are powerful for the identification of real catalytically active site in the above metioned catalyst systems, providing insights to the understanding of the active sites delicate guidance for rational design OER catalysts with high efficiency. Another challenge lies in developing a cost-effective method for the scalable fabrication of highly active electrocatalyst with high mechanical and electrochemical stabilities that could operate under high current density.

Most of present catalysts are powders and would easily peel off from the anode electrode, leading to the fast performance degradation of water splitting. Moreover, creating novel active sites with high intrinsic OER activity is also challenging but meaningful as when the intrinsic activity of an active site is high enough, twice as much can be accomplished with half the effort for improving their apparent catalytic activity.

Acknowledgements

This work was supported by the National Key Project on Basic Research (No. 2015CB932302), National Natural Science Foundation of China (No. 21773263 and No. 91645123) and the Strategic Priority Research Program of the Chinese Academy of Sciences (No. XDB12020100).

References:

[1] Lewis N S. Toward cost-effective solar energy use[J]. Science, 2007, 315(5813): 798-801.

[2] Obama B. The irreversible momentum of clean energy[J]. Science, 2017, 355(6321): 126-129.

[3] Seh Z W, Kibsgaard J, Dickens C F, et al. Combining theory and experiment in electrocatalysis: Insights into materials design[J]. Science, 2017, 355(6321): eaad4998.

[4] Gray H B. Powering the planet with solar fuel[J]. Nature Chemistry, 2009, 1(1): 7.

[5] Cook T R, Dogutan D K, Reece S Y, et al. Solar energy supply and storage for the legacy and nonlegacy worlds[J]. Chemical Reviews, 2010, 110(11): 6474-6502.

[6] Zhong Y, Xia X H, Shi F, et al. Transition metal carbides and nitrides in energy storage and conversion[J]. Advanced Science, 2016, 3(5): UNSP 1500286.

[7] Xiao P, Chen W, Wang X. A review of phosphide-based materials for electrocatalytic hydrogen evolution[J]. Advanced Energy Materials, 2015, 5(24): 1500985.

[8] Turner J A. Sustainable hydrogen production[J]. Science, 2004, 305(5686): 972-974.

[9] Suntivich J, May K J, Gasteiger H A, et al. A perovskite oxide optimized for oxygen evolution catalysis from molecular orbital principles[J]. Science, 2011, 334(6061): 1383-1385.

[10] Kanan M W, Nocera D G. *In situ* formation of an oxygen-evolving catalyst in neutral water containing phosphate and Co^{2+}[J]. Science, 2008, 321(5892): 1072-1075.

[11] Deng X, Tüysüz H. Cobalt-oxide-based materials as water oxidation catalyst: Recent progress and challenges[J]. ACS Catalysis, 2014, 4(10): 3701-3714.

[12] McCrory C C L, Jung S, Peters J C, et al. Benchmarking heterogeneous electrocatalysts for the oxygen evolution reaction[J]. Journal of the American Chemical Society, 2013, 135(45): 16977-16987.

[13] McCrory C C L, Jung S, Ferrer I M, et al. Benchmarking hydrogen evolving reaction and oxygen evolving reaction electrocatalysts for solar water splitting devices[J]. Journal of the American Chemical Society, 2015, 137 (13): 4347-4357.

[14] Jia Y, Zhang L, Gao G, et al. A heterostructure coupling of exfoliated Ni-Fe hydroxide nanosheet and defective graphene as a bifunctional electrocatalyst for overall water splitting[J]. Advanced Materials, 2017, 29(17): 1700017.

[15] Tang T, Jiang W J, Niu S, et al. Electronic and morphological dual modulation of cobalt carbonate hydroxides by Mn doping towards highly efficient and stable bifunctional electrocatalysts for overall water splitting[J]. Journal of the American Chemical Society, 2017, 139 (24): 8320-8328.

[16] Zeng M, Li Y G. Recent advances in heterogeneous electrocatalysts for the hydrogen evolution reaction[J]. Journal of Materials Chemistry A, 2015, 3(29): 14942-14962.

[17] Li J, Zheng G F. One-dimensional earth-abundant nanomaterials for water-splitting electrocatalysts[J]. Advanced Science, 2017, 4(3): 1600380.

[18] Zhuang Z C, Li Y, Li Z L, et al. MoB/g-C_3N_4 interface materials as a schottky catalyst to boost hydrogen evolution[J]. Angewandte Chemie International Edition, 2018, 57(2): 496-500.

[19] Zhang R, Wang X X, Yu S J, et al. Ternary $NiCO_2P_x$ nanowires as pH-universal electrocatalysts for highly effi cient hydrogen evolution reaction[J]. Advanced Materials, 2017, 29(9): UNSP 1605502.

[20] Chen Y Y, Zhang Y, Zhang X, et al. Self-templated fabrication of $MoNi_4/MoO_{3-x}$ nanorod arrays with dual active components for highly efficient hydrogen evolution [J]. Advanced Materials, 2017, 29(39): 1703311.

[21] Deng J, Li H B, Wang S H, et al. Multiscale structural and electronic control of molybdenum disulfide foam for highly efficient hydrogen production[J]. Nature Communications, 2017, 8: 14430.

[22] Yin Q, Tan J M, Besson C, et al. A fast soluble carbon-free molecular water oxidation catalyst based on abundant metals[J]. Science, 2010, 328(5976): 342-345.

[23] Zhao Y, Jia X, Waterhouse G I N, et al. Layered double hydroxide nanostructured photocatalysts for renewable energy production[J]. Advanced Energy Materials, 2016,

6(6): 1501974.

[24] Subbaraman R, Tripkovic D, Chang K C, et al. Trends in activity for the water electrolyser reactions on 3*d* M (Ni, Co, Fe, Mn) hydr (oxy) oxide catalysts[J]. Nature materials, 2012, 11(6): 550-557.

[25] Zhao Y, Nakamura R, Kamiya K, et al. Nitrogen-doped carbon nanomaterials as non-metal electrocatalysts for water oxidation[J]. Nature Communications, 2013, 4: 2390.

[26] Chen D, Chen C, Baiyee Z M, et al. Nonstoichiometric oxides as low-cost and highly-efficient oxygen reduction/evolution catalysts for low-temperature electrochemical devices[J]. Chemical Reviews, 2015, 115(18): 9869-9921.

[27] Song F, Hu X L. Exfoliation of layered double hydroxides for enhanced oxygen evolution catalysis[J]. Nature Communications, 2014, 5: 4477.

[28] Jiao Y, Zheng Y, Jaroniec M, et al. Design of electrocatalysts for oxygen-and hydrogen-involving energy conversion reactions[J]. Chemical Society Reviews, 2015, 44(8): 2060-2086.

[29] Long X, Li J K, Xiao S, et al. A strongly coupled graphene and FeNi double hydroxide hybrid as an excellent electrocatalyst for the oxygen evolution reaction[J]. Angewandte Chemie International Edition, 2014, 29(53): 7584-7588.

[30] Yeo B S, Bell A T. Enhanced activity of gold-supported cobalt oxide for the electrochemical evolution of oxygen [J]. Journal of the American Chemical Society, 2011, 133 (14): 5587-5593.

[31] Grimaud A, May K J, Carlton C E, et al. Double perovskites as a family of highly active catalysts for oxygen evolution in alkaline solution[J]. Nature Communications, 2013, 4: 2439.

[32] Gerken J B, McAlpin J G, Chen J Y, et al. Electrochemical water oxidation with cobalt-based electrocatalysts from pH 0-14: The thermodynamic basis for catalyst structure, stability, and activity[J]. Journal of the American Chemical Society, 2011, 133(36): 14431-14442.

[33] Li Y, Hasin P, Wu Y. $Ni_xCo_{3-x}O_4$ nanowire arrays for electrocatalytic oxygen evolution[J]. Advanced Materials, 2010, 22(17): 1926-1929.

[34] Wee T L, Sherman B D, Gust D, et al. Photochemical synthesis of a water oxidation catalyst based on cobalt nanostructures[J]. Journal of the American Chemical Society, 2011, 133(42): 16742-16745.

[35] Trotochaud L, Ranney J K, Williams K N, et al. Solution-cast metal oxide thin film electrocatalysts for oxygen evolution[J]. Journal of the American Chemical Society, 2012, 134(41): 17253-17261.

[36] Song F, Schenk K, Hu X. A nanoporous oxygen evolution catalyst synthesized by selective electrochemical etching of perovskite hydroxide $CoSn(OH)_6$ nanocubes[J]. Energy & Environmental Science, 2016, 9(2): 473-477.

[37] Tang C, Cheng N, Pu Z, et al. NiSe nanowire film supported on nickel foam: An efficient and stable 3D bifunctional electrode for full water splitting[J]. Angewandte Chemie International Edition, 2015, 54(32): 9351-9355.

[38] Liu Y, Cheng H, Lyu M, et al. Low overpotential in vacancy-rich ultrathin $CoSe_2$ nanosheets for water oxidation [J]. Journal of the American Chemical Society, 2014, 136 (44): 15670-15675.

[39] Gao M R, Xu Y F, Jiang J, et al. Water oxidation electrocatalyzed by an efficient $Mn_3O_4/CoSe_2$ nanocomposite[J]. Journal of the American Chemical Society, 2012, 134(6): 2930-2933.

[40] Zhao S, Jin R, Abroshan H, et al. Gold nanoclusters promote electrocatalytic water oxidation at the nanocluster/$CoSe_2$ interface[J]. Journal of the American Chemical Society, 2017, 139(3): 1077-1080.

[41] Zhang Y, Ouyang B, Xu J, et al. Rapid synthesis of cobalt nitride nanowires: Highly efficient and low-cost catalysts for oxygen evolution[J]. Angewandte Chemie International Edition, 2016, 55(30): 8670-8674.

[42] Guo C, Zheng Y, Ran J, et al. Engineering high-energy interfacial structures for high-performance oxygen-involving electrocatalysis[J]. Angewandte Chemie International Edition, 2017, 56(29): 8539-8543.

[43] Cui X J, Ren P J, Deng D H, et al. Single layer graphene encapsulating non-precious metals as high-performance electrocatalysts for water oxidation[J]. Energy & Environmental Science, 2016, 9(1): 123-129.

[44] Gao M R, Sheng W C, Zhuang Z B, et al. Efficient water oxidation using nanostructured α-nickel-hydroxide as an electrocatalyst[J]. Journal of the American Chemical Society, 2014, 136(19): 7077-7084.

[45] Wang J H, Cui W, Liu Q, et al. Recent progress in cobalt-based heterogeneous catalysts for electrochemical water splitting[J]. Advanced Materials, 2016, 28(2): 215-230.

[46] Chen S, Qiao S Z. Hierarchically porous nitrogen-doped graphene-$NiCO_2O_4$ hybrid paper as an advanced electrocatalytic water-splitting material[J]. ACS Nano, 2013, 7 (11): 10190-10196.

[47] Gong M, Li Y, Wang H, et al. An advanced Ni-Fe layered double hydroxide electrocatalyst for water oxidation [J]. Journal of the American Chemical Society, 2013, 135 (23): 8452-8455.

[48] Zhao Z L, Wu H X, He H L, et al. A high-performance binary Ni-Co hydroxide-based water oxidation electrode with three-dimensional coaxial nanotube array structure [J]. Advanced Functional Materials, 2014, 24(29): 4698-4705.

[49] Liu W, Liu H, Dang L N, et al. Amorphous cobalt-iron hydroxide nanosheet electrocatalyst for efficient electrochemical and photo-electrochemical oxygen evolution[J]. Advanced Functional Materials, 2017, 27(14): 1603904.

[50] Benck J D, Hellstern T R, Kibsgaard J, et al. Catalyzing the hydrogen evolution reaction (HER) with molybdenum sulfide nanomaterials[J]. ACS Catalysis, 2014, 4(11): 3957-3971.

[51] Jiang W J, Niu S, Tang T, et al. Crystallinity-modulated electrocatalytic activity of a nickel (II) borate thin layer on Ni_3B for efficient water oxidation[J]. Angewandte Chemie International Edition, 2017, 56(23): 6572-6577.

[52] Yan D F, Li Y X, Huo J, et al. Defect chemistry of non-precious-metal electrocatalysts for oxygen reactions [J]. Advanced Materials, 2017, 29(48): 1606459.

[53] Liu Y W, Xiao C, Lyu M J, et al. Ultrathin Co_3S_4 nanosheets that synergistically engineer spin states and exposed polyhedra that promote water oxidation under neutral conditions[J]. Angewandte Chemie International Edition, 2015, 54(38): 11231-11235.

[54] Xiao C L, Li Y B, Lu X Y, et al. Bifunctional porous NiFe/$NiCo_2O_4$/Ni foam electrodes with triple hierarchy and double synergies for efficient whole cell water splitting[J]. Advanced Functional Materials, 2016, 26(20): 3515-3523.

[55] Peng Z, Jia D, Al-Enizi A M, et al. From water oxidation to reduction: Homologous Ni-Co based nanowires as complementary water splitting electrocatalysts[J]. Advanced Energy Materials, 2015, 5(9): 1402031.

[56] Zheng Y R, Gao M R, Gao Q, et al. An efficient CeO_2/$CoSe_2$ nanobelt composite for electrochemical water oxidation[J]. Small, 2015, 11(2): 182-188.

[57] Indra A, Menezes P W, Sahraie N R, et al. Unification of catalytic water oxidation and oxygen reduction reactions: Amorphous beat crystalline cobalt iron oxides[J]. Journal of the American Chemical Society, 2014, 136(50): 17530-17536.

[58] Lukowski M A, Daniel A S, Meng F, et al. Enhanced hydrogen evolution catalysis from chemically exfoliated metallic MoS_2 nanosheets[J]. Journal of the American Chemical Society, 2013, 135(28): 10274-10277.

[59] Chen P Z, Xu K, Tao S, et al. Phase-transformation engineering in cobalt diselenide realizing enhanced catalytic activity for hydrogen evolution in an alkaline medium[J]. Advanced Materials, 2016, 28(34): 7527-7532.

[60] Li H, Shang J, Ai Z H, et al. Efficient visible light nitrogen fixation with biobr nanosheets of oxygen vacancies on the exposed {001} facets[J]. Journal of the American Chemical Society, 2015, 137(19): 6393-6399.

[61] Bao J, Zhang X D, Fan B, et al. Ultrathin spinel-structured nanosheets rich in oxygen deficiencies for enhanced electrocatalytic water oxidation[J]. Angewandte Chemie International Edition, 2015, 25(54): 7399-7404.

[62] Wang Y C, Zhou T, Jiang K, et al. Reduced mesoporous Co_3O_4 nanowires as efficient water oxidation electrocatalysts and supercapacitor electrodes[J]. Advanced Energy Materials, 2014, 4(16): 1400696.

[63] Tong Y, Guo Y Q, Chen P Z, et al. Spin-state regulation of perovskite cobaltite to realize enhanced oxygen evolution activity[J]. Chem, 2017, 3(5): 812-821.

[64] Huang J H, Chen J T, Yao T, et al. CoOOH nanosheets with high mass activity for water oxidation[J]. Angewandte Chemie International Edition, 2015, 54(30): 8722-8727.

[65] Su C Y, Cheng H, Li W, et al. Atomic modulation of Fe-Co-nitrogen-carbon bifunctional oxygen electrodes for rechargeable and flexible all-solid-state zinc-air battery [J]. Advanced Energy Materials, 2017, 7(13): 1602420.

[66] Fu G T, Yan X X, Chen Y F, et al. Boosting bifunctional oxygen electrocatalysis with 3*d* graphene aerogel-supported Ni/MnO particles[J]. Advanced Materials, 2018, 30(5): 1704609.

[67] Liang Y Y, Li Y G, Wang H L, et al. Co_3O_4 nanocrystals on graphene as a synergistic catalyst for oxygen reduction reaction[J]. Nature Materials, 2011, 10(10): 780-786.

[68] Zhong D K, Sun J, Inumaru H, et al. Solar water oxidation by composite catalyst/α-Fe_2O_3 photoanodes[J]. Journal of the American Chemical Society, 2009, 131(17): 6086-6087.

[69] Chen Z P, Ren W C, Gao L B, et al. Three-dimensional flexible and conductive interconnected graphene networks grown by chemical vapour deposition[J]. Nature Materials, 2011, 10(6): 424-428.

[70] Yong Y C, Dong X C, Chan-Park M B, et al. Macroporous and monolithic anode based on polyaniline hybridized three-dimensional graphene for high-performance microbial fuel cells[J]. ACS Nano, 2012, 6(3): 2394-2400.

[71] Dong X C, Xu H, Wang X W, et al. 3*d* graphene-cobalt oxide electrode for high-performance supercapacitor and enzymeless glucose detection[J]. ACS Nano, 2012, 6(4): 3206-3213.

[72] Wu Z S, Zhou G, Yin L C, et al. Graphene/metal oxide

composite electrode materials for energy storage[J]. Nano Energy, 2012, 1(1): 107-131.

[73] Miao R, He J K, Sahoo S, et al. Reduced graphene oxide supported nickel-manganese-cobalt spinel ternary oxide nanocomposites and their chemical-converted sulfide nanocomposites as efficient electrocatalysts for alkaline water splitting[J]. ACS Catalysis, 2017, 7(1): 819-832.

[74] Guo Y X, Gan L F, Shang C S, et al. A cake-style CoS_2@MoS_2/rGO hybrid catalyst for efficient hydrogen evolution[J]. Advanced Functional Materials, 2017, 27(5): UNSP 1602699.

[75] Tang T, Jiang W J, Niu S, et al. Kinetically controlled co-precipitation for general fast synthesis of sandwiched metal hydroxide nanosheets/graphene composites toward efficient water splitting[J]. Advanced Functional Materials, 2018, 28(3): 1704594.

[76] Chen P Z, Xu K, Zhou T P, et al. Strong-coupled cobalt borate nanosheets/graphene hybrid as electrocatalyst for water oxida tion under both alkaline and neutral conditions[J]. Angewandte Chemie International Edition, 2016, 55(7): 2488-2492.

[77] Frydendal R, Paoli E A, Knudsen B P, et al. Benchmarking the stability of oxygen evolution reaction catalysts: The importance of monitoring mass losses[J]. ChemElectroChem, 2014, 1(12): 2075-2081.

[78] Hellstern T R, Benck J D, Kibsgaard J, et al. Engineering cobalt phosphide (CoP) thin film catalysts for enhanced hydrogen evolution activity on silicon photocathodes[J]. Advanced Energy Materials, 2016, 6(4): 1501758.

[79] Niu S, Jiang W J, Tang T, et al. Facile and scalable synthesis of robust $Ni(OH)_2$ nanoplate arrays on NiAl foil as hier archical active scaffold for highly efficient overall water splitting[J]. Advanced Science, 2017, 4(8): 1700084.

[80] Zhang W, Qi J, Liu K Q, et al. A nickel-based integrated electrode from an autologous growth strategy for highly efficient water oxidation[J]. Advanced Energy Materials, 2016, 6(12): 1502489.

[81] Jin S. Are metal chalcogenides, nitrides, and phosphides oxygen evolution catalysts or bifunctional catalysts? [J]. ACS Energy Letters, 2017, 2(8): 1937-1938.

[82] Xu K, Cheng H, Liu L Q, et al. Promoting active species generation by electrochemical activation in alkaline media for efficient electrocatalytic oxygen evolution in neutral media[J]. Nano Letters, 2017, 17(1): 578-583.

高性能析氧电催化剂的设计策略

唐 堂,江文杰,牛 帅,胡劲松*

(中国科学院化学研究所, 中国科学院分子纳米结构与纳米技术重点实验室, 北京 100190)

摘要: 电催化水分解反应是可以实现规模化制取氢气的一种重要绿色无污染的手段, 但是其效率极大地受制于阳极析氧反应. 因此,发展廉价、高效的析氧反应催化剂是当下的研究热点. 通过分析决定析氧反应催化活性的因素,本综述总结了低成本、高效、稳定的析氧电催化剂的一些通用设计与制备策略,包括:1)通过电子结构调控、结晶度调控、相调控、缺陷位调控以及自旋态调控提升单个催化活性位点的本征催化活性;2)设计与构筑先进电极结构,以实现活性位点数量最大化,获得大电流下稳定的电极材料. 进而,选取了一些具有代表性的高效析氧催化剂作为例子来阐述这些策略的实用性. 最后,对高效、可在大电流密度下稳定工作的析氧催化剂的理性设计、可控制备和发展方向提出了展望,以期为新型高性能析氧催化剂的设计提供指导.

关键词: 析氧反应;电解水;电催化剂;设计策略;制氢